scientific reports

Check for updates

OPEN

Diplexer based microwave sensor for noninvasive detection of sucrose and sorbitol in pharmaceutical syrups

Seyed Abed Zonouri✉, Saeed Mehdipourbashi & Mazdak Rad Malekshahi

In this study, a novel low-pass/band-pass diplexer-based microwave sensor is introduced for the first time as a high-sensitivity platform for the detection and quantification of sucrose and sorbitol concentrations in pharmaceutical syrups. The proposed sensor features a compact footprint of 13.1 mm × 15.84 mm and integrates two distinct filtering paths, each optimized for specific spectral ranges. The band-pass and low-pass filters are constructed using a combination of M-notch-shaped and semicircular-shaped resonators, with the latter enhanced by integrated spiral lines to reduce both physical dimensions and resonant frequency. This geometric optimization enables stronger field confinement and improved sensitivity. An equivalent lumped-element LC circuit model is also presented to accurately predict the resonators' behavior and validate the electromagnetic performance. The sensor's functionality was experimentally verified using three commercially available pharmaceutical syrups—Diphenhydramine, Guaifenesin, and Salbutamol—each with varying concentrations of sweetening agents. The sensor achieved a maximum sensitivity of 9312.5 MHz/(g mL^{-1}) and a minimum detection limit (DL) of 0.00037 (dB g)/(MHz mL), demonstrating exceptional accuracy in resolving small dielectric variations. The observed nonlinear correlation between sweetener concentration and resonant frequency shift enables precise quantification of both sucrose and sorbitol across diverse formulations. The combination of high sensitivity, excellent repeatability, and miniaturized design makes the proposed sensor highly suitable for real-time, non-invasive quality control of pharmaceutical syrups. This work represents a significant advancement in dielectric-based sensing and offers promising potential for implementation in both laboratory testing and point-of-care diagnostics within the pharmaceutical industry.

Keywords Dielectric characterization, Diplexer based sensing, Microwave sensor, Pharmaceutical syrup, Sucrose and sorbitol detection

Microwave structures are critical components in modern communication systems and sensing applications. These structures are designed to manipulate electromagnetic signals, enabling precise control over frequency, power, and signal distribution[1–3]. Among the most prominent microwave structures are power dividers[4–6], filters[7], diplexers[8,9], triplexers[10], and couplers[11,12], each serving specific roles. Power dividers are used to split or combine signals, ensuring equal or unequal power distribution. Filters are employed to pass signals within a desired frequency range while attenuating others, with common variants including low-pass, high-pass, band-pass, and band-stop filters. Diplexers and triplexers are advanced structures that allow simultaneous transmission or reception of signals in two or three distinct frequency bands, respectively, enabling more complex and efficient system designs.

Microwave sensors have emerged as a transformative technology for non-invasive, real-time, and high-precision measurements across various industries, including healthcare, environmental monitoring, and telecommunications. Their ability to detect subtle changes in material properties, such as permittivity and conductivity, makes them ideal for applications requiring precise parameter estimation. In the pharmaceutical industry, where quality control is critical, microwave sensors offer significant advantages over traditional chemical methods in terms of speed, accuracy, and repeatability[13,14].

Department of Electrical Engineering, Faculty of Engineering, Razi University, Kermanshah, Iran. ✉email: a.zonoori@yahoo.com

Among the available microwave structures, diplexers hold a unique position in sensing applications due to their dual-band functionality. Unlike single-band sensors, diplexers enable measurement in at least two distinct frequency bands, providing the flexibility to monitor multiple parameters simultaneously. This multi-band capability extends the application range of diplexers beyond conventional sensors, making them an ideal choice for scenarios requiring comprehensive and simultaneous analysis of diverse parameters.

In[15], a paper presents a highly sensitive microwave sensor for dielectric sensing. This work eliminates unwanted errors by using a differential measurement technique by comparing two resonant transmission frequencies during a single test setup to measure the material under test (MUT) permittivity over time. The proposed structure consists of a helical resonator with an extended horizontal microstrip line (EH-ML) coupled to a microstrip transmission line. This structure suffers from large dimensions and complex structure.

Ref.[16] presents a highly sensitive and compact non-invasive microwave sensor for real-time blood glucose measurement. The authors have developed a novel sensing technique using branch line couplers and split-ring resonators. On the other hand, Ref.[17] introduces a novel metamaterial absorber featuring a dumbbell-shaped, modified circular ring resonator, designed for applications in S, X, and Ku band microwave sensing. The design incorporates rotational symmetry and surface current analysis to ensure polarization insensitivity and robust absorption. By leveraging equivalent circuit modeling and CST simulations, the proposed absorber demonstrates exceptional performance, making it suitable for liquid sensing and other electromagnetic applications.

Recent developments in resonator-based microwave sensors have successfully mitigated traditional challenges associated with large structural footprints, limited frequency bandwidth, and complex fabrication processes. Notably, the design of quad-band split-ring resonator sensors with compact 8×8 mm^2 dimensions has enabled high sensitivity and reliability across multiple frequency bands, achieving efficient microwave sensing without added circuit complexity[18]. Additionally, advances in differential microstrip sensors utilizing LC resonators have demonstrated significant improvements in complex permittivity measurements of liquid media, achieving average sensitivity enhancements of 2.53% while maintaining minimal structural dimensions[19]. These innovations reflect a broader trend towards miniaturized and highly efficient sensor designs capable of precise permittivity characterization. Further progress in battery-free microwave sensors has also contributed to entirely passive operation modes with heightened sensitivity, eliminating the need for intricate power management mechanisms and paving the way for sustainable, low-maintenance sensing applications[20].

Although recent advancements in microwave sensor technology have made significant strides in miniaturization and sensitivity optimization, persistent challenges—including bulky structural designs, constrained frequency band coverage, and intricate fabrication processes—continue to limit their scalability in compact, multi-analyte pharmaceutical applications. Addressing these limitations, this study presents an innovative low-pass/band-pass diplexer-based microwave sensor engineered specifically for the simultaneous detection of sucrose and sorbitol concentrations in popular pharmaceutical syrups such as Diphenhydramine, Guaifenesin, and Salbutamol. The proposed design not only overcomes the barriers of size and complexity but also enhances multi-band operability within a singular, streamlined platform, setting a new benchmark for real-time, non-invasive quality control in pharmaceutical monitoring.

The proposed diplexer structure distinguishes itself through its miniaturized multi-analyte design, occupying only 13.1 mm $\times$ 15.84 mm, and its high sensitivity, reaching a maximum value of 9312.5 ($\frac{\text{MHz}}{\text{gr/mL}}$), which allows for the precise discrimination of small variations in analyte concentrations. By leveraging the multi-band nature of the diplexer, the sensor effectively isolates and monitors responses in multi distinct frequency ranges, enabling multi-parameter analysis within a single compact platform. Furthermore, the design's simplicity and compatibility with standard planar fabrication techniques ensure its applicability in real-world scenarios, particularly in pharmaceutical quality control where real-time, non-invasive, and accurate measurement is critical. This study presents the design, simulation, and performance evaluation of the sensor, highlighting its advantages and practical utility in pharmaceutical monitoring applications.

Diplexer design

A diplexer is a passive microwave component used to separate or combine signals in two distinct frequency bands, allowing simultaneous transmission or reception through a single input port. By directing different frequency ranges to different output paths, diplexers play a critical role in communication systems and sensing applications that require multi-band operation[21,22].

The diplexer presented in this study is designed for dual-band sensing and is composed of two distinct filter sections: a low-pass filter (LPF) and a band-pass filter (BPF), as illustrated in Fig. 1. The LPF is responsible for passing lower frequencies, while the BPF allows middle frequencies to reach the output, enabling the structure to operate effectively across a wide frequency range.

This dual-filter configuration allows the sensor to detect variations in the dielectric properties of different materials—specifically sucrose and sorbitol in pharmaceutical syrups—at separate frequency bands. The design offers high selectivity, low insertion loss, and small size, making it well-suited for real-time and non-invasive monitoring applications.

BPF design

The BPF section of the proposed diplexer is realized using novel M-notch-shaped resonators, which provide a ultra-small size, high selectivity, and strong electromagnetic field confinement. These resonators are specifically engineered to support a well-defined passband in the mid-frequency range, enabling accurate detection of changes in the dielectric properties of the MUT.

The layout of a single M-notch-shaped resonator is illustrated in Fig. 2a. The structure features a semi-circular top profile with two inward-facing triangular notches that form a distinctive "M" shape, enhancing localized

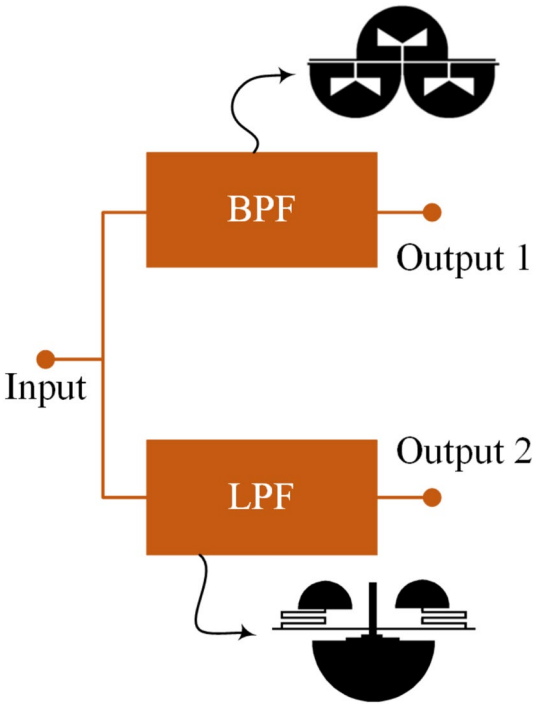

Fig. 1. Layout of the proposed diplexer with integrated LPF and BPF.

field distribution and improving sensing sensitivity. The symmetrical geometry allows for efficient coupling and compact integration into the filter network.

In the resonator layout illustrated in Fig. 2a, the geometric parameters of the structure are defined as follows: A1 = 3 mm, A2 = 1.61 mm, A3 = 1.7 mm, A4 = 0.89 mm, A5 = 0.17 mm, and A6 = 1.25 mm, corresponding to the key structural features of the M-notch-shaped resonator. So, to better understand and model the resonator's behavior, an equivalent inductor-capacitor (LC) circuit is derived, as shown in Fig. 2b. This equivalent circuit is constructed based on the modeling approach presented in Ref.[2,23,24], where the resonator's electromagnetic response is mapped to lumped circuit elements. The values of the inductors and capacitors in this model represent the distributed inductance and capacitance of the resonator arms and gaps.

The element values in the LC model can be analytically estimated using a set of closed-form expressions provided in Eqs. (1)–(6). These equations relate the physical dimensions of the resonator to its resonant frequency and impedance characteristics, enabling accurate prediction and tuning of the filter's performance without extensive numerical optimization. The following set of equations, derived from transmission line theory and discussed in[2,25], allows for the analytical calculation of these equivalent parameters based on physical and material characteristics.

The equivalent capacitance C per unit length can be estimated using:

$$capacitororC = \left[8.85 \times 10^{-12} \times \left\{\left[\frac{\varepsilon_r \times w}{h}\right]^{1.08} + \left[2\pi\left(\frac{\varepsilon_r + 1}{2}\right) \times \left(\frac{1}{\ln\left(\frac{8h}{w} + 1\right)} - \frac{w}{8h}\right)\right]^{1.08}\right\}^{0.926}\right] \times l \quad (1)$$

The inductance L per unit length can be obtained using:

$$L = \frac{Z \times l}{V_p}, V_p = \frac{c_0}{\sqrt{\varepsilon_{re}}} \quad (2)$$

Here, Z is the characteristic impedance, V_p is the phase velocity, and $c_0 = 3 \times 10^8 m/s$ is the speed of light in vacuum. The effective relative permittivity ε_{re} and the characteristic impedance Z depend on the ratio w/h (line width to substrate height) and are calculated differently for narrow and wide traces:

For $w/h \leq 1$:

$$\varepsilon_{re} = \frac{\varepsilon_r + 1}{2} + \frac{\varepsilon_r - 1}{2} \times \left\{\frac{1}{\sqrt{\left[1 + 12\frac{h}{w}\right]}} + 0.04\left[1 - \frac{w}{h}\right]^2\right\} \quad (3)$$

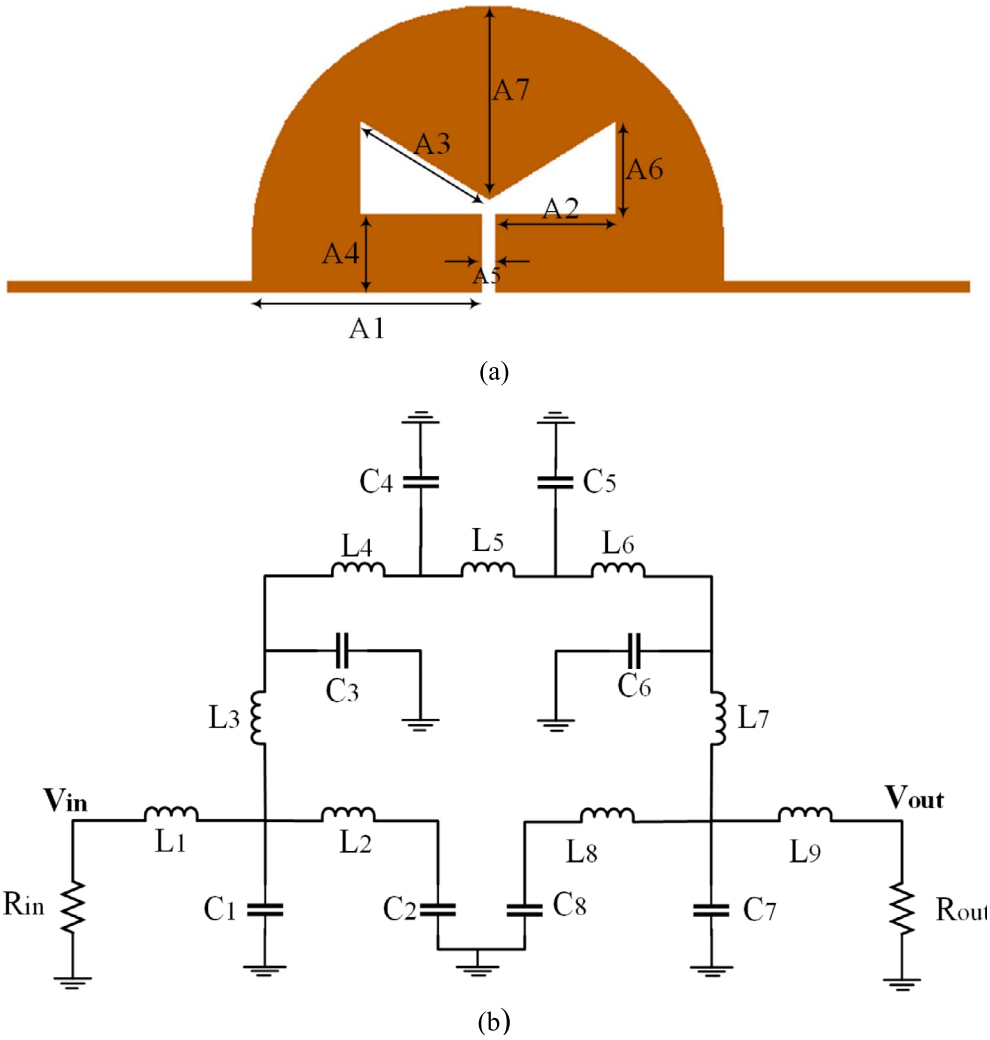

Fig. 2. (**a**) Geometric layout of the proposed M-notch-shaped resonator, and (**b**) LC equivalent circuit model.

$$Z = \frac{\eta}{2\pi\sqrt{\varepsilon_{re}}} \times \ln\left[8\frac{h}{w} + 0.25\frac{w}{h}\right] \tag{4}$$

For $w/h \geq 1$:

$$\varepsilon_{re} = \frac{\varepsilon_r + 1}{2} + \frac{\varepsilon_r - 1}{2}\left\{\left[1 + 12\frac{h}{w}\right]^{-0.5}\right\} \tag{5}$$

$$Z = \frac{\eta}{\sqrt{\varepsilon_{re}}} \times \{\frac{h}{w} + 1.393 + 0.677 \times \ln\left[\frac{w}{h} + 1.444\right]\}^{-1} \tag{6}$$

In these equations:

- ε_r is the substrate's relative permittivity,
- ε_{re} is the effective dielectric constant,
- $\eta \approx 377\ \Omega$ is the intrinsic impedance of free space,
- w, h, and l are the width, height (thickness), and length of the microstrip line, respectively.

These equations enable the estimation of the microstrip line's equivalent inductance and capacitance for a given substrate. As a result, the behavior of complex resonator structures—such as the M-notch-shaped resonator introduced in this work—can be effectively modeled and analyzed in terms of lumped elements, facilitating the design and optimization of microwave filters and sensors.

The designed M-notch-shaped resonator is simulated on an FR4 substrate, which has a relative permittivity of $\varepsilon_r = 4.4$, a loss tangent of 0.0022, and a thickness of 1.6 mm. Based on the known physical dimensions of the resonator and the substrate characteristics, the values of the equivalent inductors and capacitors are extracted

L_1	L_2	L_3	L_4	L_5	L_6	L_7	L_8	L_9
4.25	1.08	0.49	1.87	2.04	1.87	0.49	1.08	4.25
C_1	C_2	C_3	C_4	C_5	C_6	C_7	C_8	
0.76	0.054	0.06	0.91	0.91	0.06	0.76	0.054	

Table 1. Equivalent inductor and capacitor values for the presented resonator (unit: nH, pF).

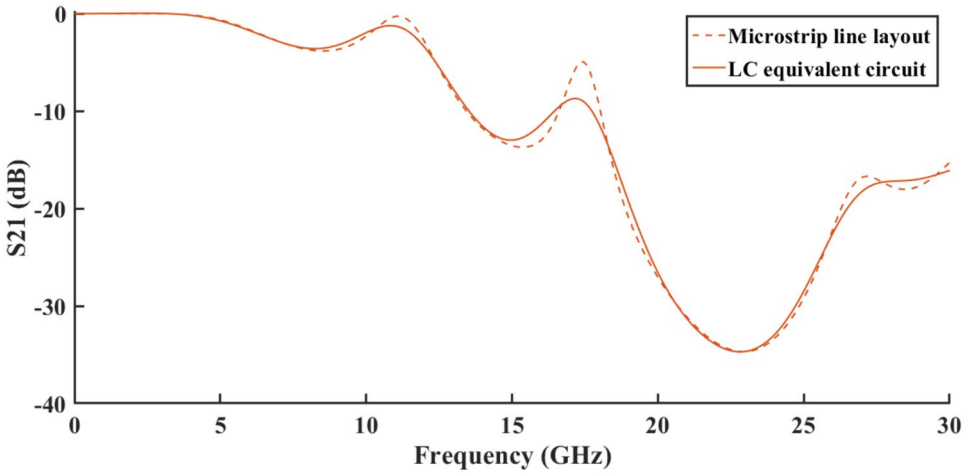

Fig. 3. Comparison of simulation results of microstrip line and its equivalent LC circuit.

using the analytical relations presented in Eqs. (1)–(6). These calculations enable an accurate representation of the resonator's electromagnetic behavior through its lumped-element model. The detailed geometric parameters used in the simulation are listed in Table 1.

After determining the values of all equivalent inductors and capacitors, the voltage gain of the circuit—defined as the ratio Vo/Vin—can be analytically calculated by applying Kirchhoff's Voltage Law (KVL) and Kirchhoff's Current Law (KCL) to the lumped-element model. These laws are used to evaluate the relationships among the series and parallel combinations of the reactive components, allowing accurate prediction of the circuit's frequency response.

In Fig. 3, the simulated S21-parameter response of the physical M-notch-shaped resonator is compared with the response of its corresponding LC equivalent circuit. As observed, the two responses exhibit excellent agreement, with only a slight deviation. This minor discrepancy is attributed to parasitic coupling capacitances between adjacent microstrip lines in the physical layout—effects that are typically neglected in the lumped-element model due to their relatively small magnitude. The close match between the two responses validates the accuracy of the derived equivalent circuit and confirms its suitability for modeling the resonator's behavior.

As illustrated in Fig. 3, the proposed M-notch-shaped resonator does not exhibit optimal performance in a low-pass configuration. However, since the intended application is for a BPF, the resonator was incorporated into a band-pass structure and further evaluated. Figure 4a–c illustrate the geometric layouts of the one, three, and five resonator configurations, respectively. The initial choice of a single resonator, as depicted in Fig. 4a, is based on the fundamental M-notch integrated semicircular structure, serving as the primary field-confinement mechanism. This design establishes the baseline electromagnetic response for subsequent configurations. Figure 4b extends the architecture by introducing three resonators in a symmetric arrangement, enhancing electromagnetic coupling and expanding bandwidth. This design follows the modular principles derived from the primary structure, with calculated spacing to optimize field interaction and phase integrity. In Fig. 4c, the configuration is further extended to five resonators, strategically aligned to maximize bandwidth and sensitivity through denser field confinement. However, the increased complexity introduces potential spectral overlap, which requires careful consideration in practical applications. Finally, Fig. 4d presents the simulated S21 responses for all configurations, demonstrating progressive improvements in bandwidth and resonance sharpness with the addition of resonators.

The results reveal that the configuration employing three resonators yields the most favorable performance. Specifically, this design achieves two well-defined passbands, with significantly reduced S21 values in the stopbands and minimal insertion loss within the passbands. Moreover, the transition regions exhibit increased sharpness, indicating enhanced selectivity—an essential characteristic for effective BPF operation. The designed BPF with 3 M-notch-shaped resonators exhibits two distinct passbands centered at 2.1 GHz and 3.8 GHz, respectively. The first passband offers a bandwidth of approximately 385 MHz, while the second passband provides a bandwidth of about 290 MHz, indicating the filter's capability to support multi-band operation with well-defined spectral characteristics.

(a)

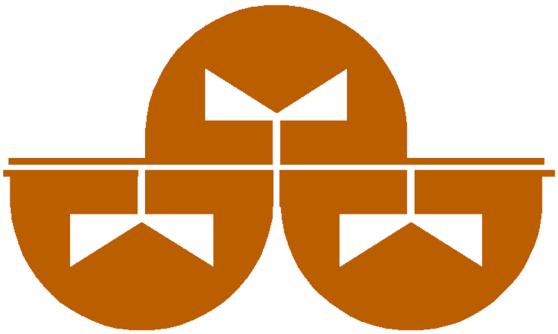

(b)

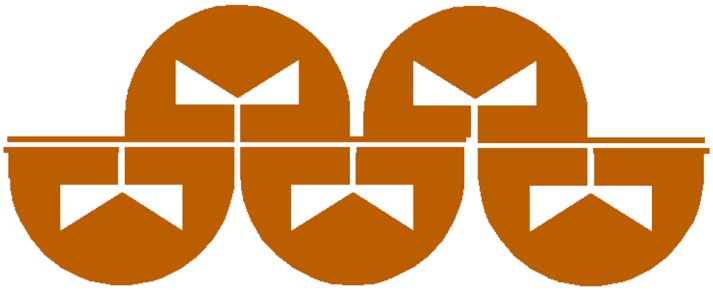

(c)

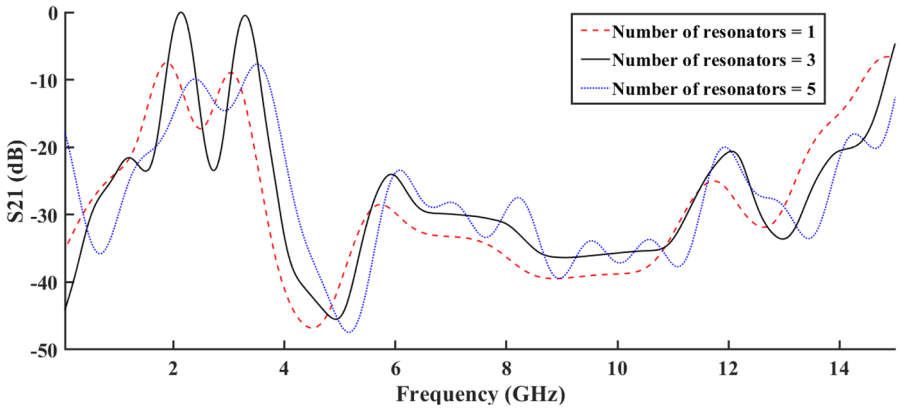

(d)

Fig. 4. BPF structure with (**a**) one resonator, (**b**) three resonators, (**c**) five resonators, and (**d**) simulated S21 results for all configurations.

Therefore, based on the superior spectral performance demonstrated in Fig. 4d, the configuration with three M-notch-shaped resonators is selected for integration into the final diplexer design.

LPF design

To design the LPF section of the final diplexer, semicircular-shaped resonators are employed due to their favorable frequency response characteristics, as demonstrated in[2,26]. Also, to address the compactness requirements and

minimize the overall footprint of the device, spiral transmission lines are incorporated into the base of the semicircular-shaped resonator. This design approach results in a compact and efficient structure, as illustrated in Fig. 5a.

To evaluate the impact of spiral line length on the resonator's performance, three configurations—featuring short, medium, and long spiral lines—are analyzed. The corresponding layouts and simulated S21-parameter responses are presented in Fig. 5b. The simulation results reveal a clear trend: as the length of the spiral line increases, the effective electrical length of the resonator grows, leading to a lower resonance frequency. Conversely, shorter spiral lines produce higher resonance frequencies. This behavior confirms the tunability of the resonator through geometric variation, enabling the precise adjustment of the LPF's frequency characteristics while maintaining a compact design.

Considering the objective of designing a diplexer with combined band-pass/low-pass functionality, and given that the passbands of the BPF are centered at 2.1 GHz and 3.8 GHz, it is essential that the low-pass section does not interfere with these operational bands. Based on the simulation results, the long spiral-line resonator is identified as the most suitable configuration for the LPF. This design exhibits a cutoff frequency of approximately 1.68 GHz, which effectively isolates it from the band-pass region and ensures minimal interference with the higher frequency passbands, thereby supporting the proper operation of the diplexer.

On the other hand, to enhance the low-pass performance of the proposed structure—specifically to increase the cutoff bandwidth and suppress higher-order harmonics—a modified configuration is employed. As illustrated in Fig. 6a, the design incorporates two symmetrical semicircular resonators with an open-ended stub placed between them. This configuration contributes to improved harmonic rejection and sharper transition characteristics.

Furthermore, to optimize the filter's performance within the passband—by reducing insertion loss, minimizing return loss, and further extending the cutoff bandwidth—a larger semicircular resonator is introduced. This resonator is composed of three impedance sections, labeled Z1, Z2, and Z3, strategically arranged to balance

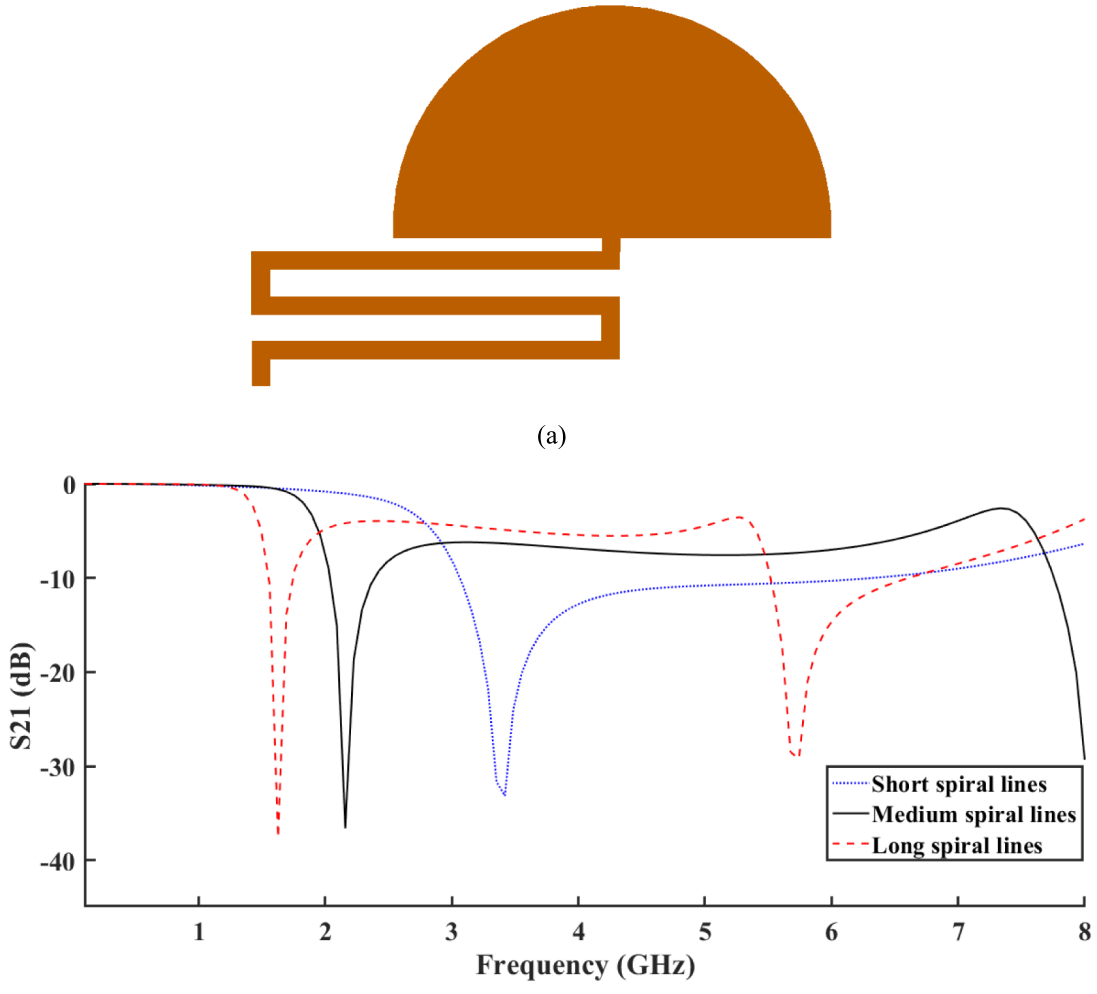

Fig. 5. (**a**) Layout of the proposed semicircular resonator with integrated spiral lines, (**b**) comparison of simulated S21 for short, medium, and long spiral configurations.

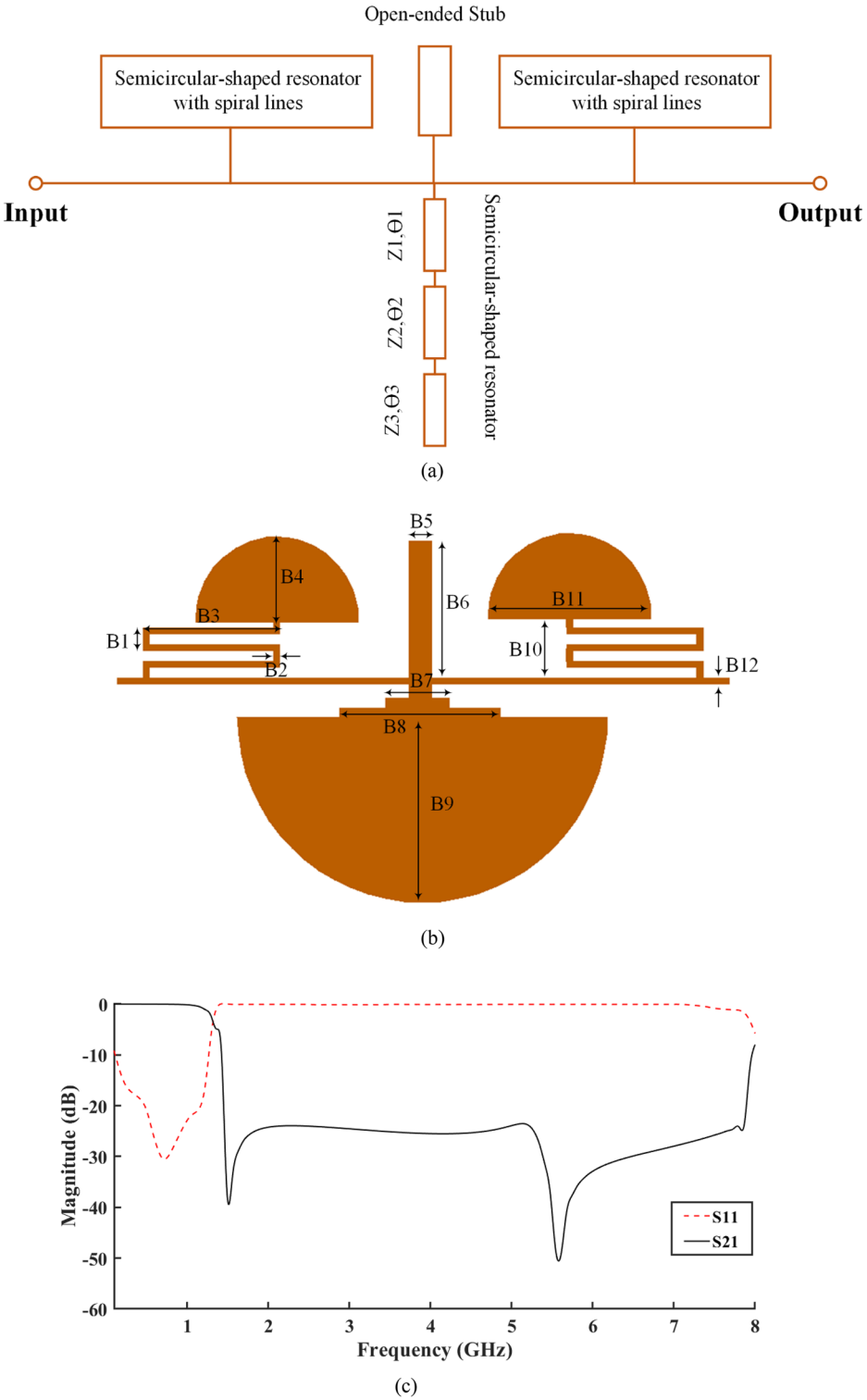

Fig. 6. (**a**) Schematic configuration of the proposed LPF, (**b**) physical layout incorporating semicircular-shaped and open-ended stub, (**c**) simulated S-parameters results.

the electromagnetic field distribution and improve impedance matching. The final layout of the LPF, integrating these enhancements, is shown in Fig. 6b. The corresponding physical dimensions are specified as: B1 = 0.45, B2 = 0.11, B3 = 2.8, B4 = 1.75, B5 = 0.46, B6 = 2.84, B7 = 1.3, B8 = 3.3, B9 = 4, B10 = 1.2, B11 = 3.38 and B12 = 0.11 (unit: mm). On the other hand, Fig. 6c shows the simulated S-parameters results of the designed filter.

The geometric parameters of the diplexer—such as the dimensions of the M-notch resonators, the spacing between resonators, and the length of spiral lines—were optimized through a parametric sweep-

based electromagnetic simulation approach using Advanced Design System (ADS) software. In this process, key parameters were systematically varied within predefined ranges to evaluate their impact on S-parameter responses, resonant frequencies, and electromagnetic field confinement. Although no metaheuristic algorithms (e.g., PSO, GA) were used in this study, the iterative parametric optimization method allowed for a fine-tuned balance between compactness, bandwidth, and sensitivity. The design objective was to maximize the sensor's response (i.e., resonant frequency shift) to small changes in the dielectric constant of the MUT, while minimizing insertion loss and maximizing field concentration in the sensing region.

The geometric optimization of the proposed diplexer has a direct influence on its sensitivity characteristics. Specifically, refinements to the resonator structures—such as the shaping of the M-notch profiles and the adjustment of the spiral line lengths—result in improved electromagnetic field confinement. This enhanced localization of the electric field within the sensing region leads to a stronger interaction with the MUT, thereby increasing the sensor's responsiveness to variations in dielectric properties. Furthermore, precise dimensional tuning ensures adequate spectral separation between the low-pass and band-pass paths, which reduces spectral overlap and improves the accuracy of detecting frequency shifts associated with different analytes. In addition, optimization of resonator spacing and impedance transitions contributes to lower insertion losses across the operational bands. This reduction in signal attenuation enhances the signal-to-noise ratio, thereby supporting more accurate and repeatable detection of subtle permittivity changes. Collectively, these design considerations play a central role in achieving the high sensitivity observed in the proposed microwave sensor.

Final layout of the proposed diplexer

The final layout of the designed low-pass/band-pass diplexer is presented in Fig. 7a. The overall footprint of the circuit is compact, measuring only 13.1 mm × 15.84 mm, and it is fabricated on an FR4 substrate with a thickness of 1.6 mm, as shown in Fig. 7b. For effective power transmission and impedance matching, three 50-Ω SMA connectors are soldered at the input and output ports.

The simulated and measured S-parameter results of the fabricated diplexer is shown in Fig. 7c. The measurement results confirm the expected band-pass behavior at Port 2, exhibiting two distinct passbands centered at 1.48 GHz and 2.15 GHz. At these frequencies, the return losses are measured at approximately – 22.1 dB and – 23.5 dB, respectively, indicating excellent impedance matching. The corresponding fractional bandwidths (FBW) are calculated to be 17.45% and 14.6%, respectively. Furthermore, the measurement results demonstrate effective harmonic suppression, with no significant spurious responses observed up to 8 GHz, which was the upper limit of the measurement range. This validates the diplexer's ability to maintain a clean spectral profile and a wide cutoff bandwidth.

In parallel, Port 3 exhibits the intended low-pass behavior, with a transmission bandwidth extending up to 1.22 GHz. Across this range, the return loss remains below – 17 dB, corresponding to an FBW of approximately 48.4%, which is highly desirable for LPF performance. Minor discrepancies between the measured and simulated results (obtained using ADS software) are observed. These differences are attributed to practical factors such as fabrication tolerances, measurement uncertainties, and imperfect calibration during the measurement process.

A comprehensive comparison of the proposed diplexer-based microwave sensor with previously reported designs is provided in Table 2, highlighting essential performance metrics, including operating frequency, structural configuration, FBW, insertion loss (|S21|), return loss (|S11|), and device size. This comparative analysis underscores the proposed sensor's significant advancements in terms of miniaturization, enhanced bandwidth, and optimized loss parameters.

The proposed diplexer achieves an innovative structural design that allows for both LP and BP filtering within a highly compact form factor of 13.1 mm × 15.84 mm. This optimized footprint is notably smaller than many conventional designs reported in the literature. For example, Ref.[27] employs a BP/BP configuration with a footprint exceeding 92.8 mm × 33.1 mm, which is nearly six times larger than the proposed sensor. Despite its size, the design in[27] demonstrates limited bandwidth and higher insertion losses, indicating suboptimal electromagnetic field confinement. In contrast, the proposed diplexer not only minimizes physical space but also achieves superior frequency isolation for both LP and BP operations. The design presented in[28] features a BP/BP configuration operating across a wide frequency spectrum. However, despite its larger size of 19.5 mm × 21.1 mm, it exhibits higher insertion losses and narrower bandwidths compared to the proposed design. Notably, the proposed diplexer attains significantly wider FBW for both the low-pass and band-pass paths, ensuring robust multi-band coverage with minimal signal degradation. This enhanced bandwidth directly translates to improved sensitivity and more effective signal transmission in multi-analyte pharmaceutical detection.

Similarly, Ref.[29] introduces a BP/LP structure with individual paths for low-pass and band-pass operations. However, the footprint of 48 mm × 46 mm is markedly larger than the proposed sensor, which is optimized to fit within a far smaller area while maintaining superior bandwidth and lower insertion loss. The design in[29] also displays considerably higher insertion losses, reflecting less efficient field confinement and higher signal attenuation. The proposed diplexer addresses these limitations through a refined resonator design, enhancing field coupling and minimizing energy dissipation.

In[30], the BP/LP configuration is further explored, but it still occupies 24.9 mm × 33.9 mm of real estate—almost three times the size of the proposed design. Furthermore, the insertion loss values are considerably higher, indicating signal degradation that the proposed diplexer effectively mitigates. This is achieved by leveraging M-notch and semicircular resonators that optimize electromagnetic field distribution, enhancing both return loss and insertion loss parameters. Also, the diplexer in[31] operates at mid-range frequencies with a BP/BP configuration but sacrifices footprint efficiency with a 24 mm × 18 mm structure. While it achieves acceptable return loss values, the insertion loss remains above optimal levels for precision sensing applications. Conversely, the proposed diplexer significantly reduces insertion loss to as low as 0.7 dB for the low-pass path, ensuring cleaner signal propagation and enhanced sensitivity for non-invasive analyte detection. Furthermore,

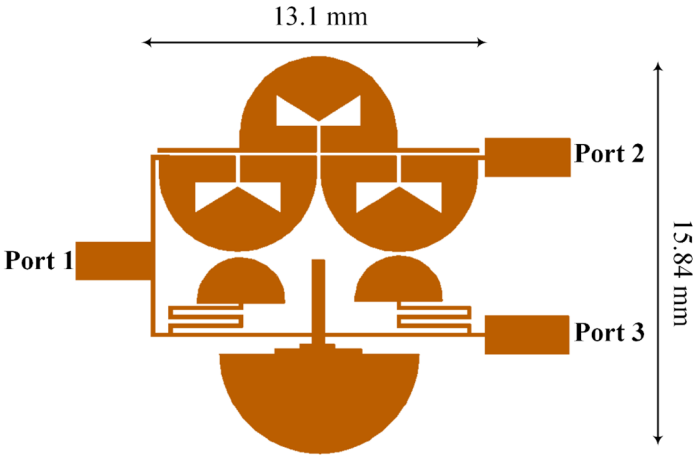

(a)

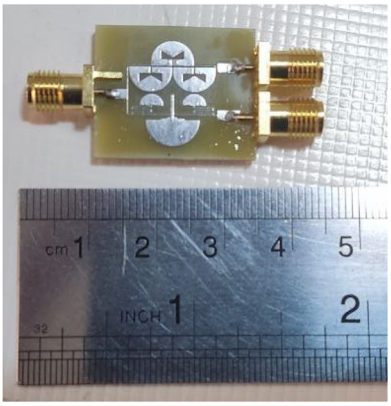

(b)

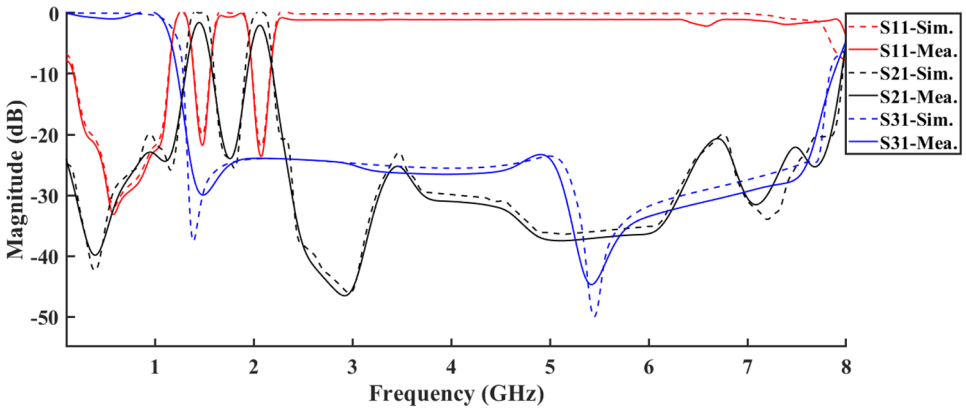

(c)

Fig. 7. (**a**) Layout of the proposed low-pass/band-pass diplexer, (**b**) fabricated prototype on FR4 substrate, and (**c**) simulated and measured S-parameters.

Ref.[32] introduces another BP/BP design with a 32 mm × 26 mm layout, which, although effective for general dielectric monitoring, lacks the multi-band flexibility and optimized loss parameters of the proposed design. The larger footprint and higher insertion losses highlight its limitations in high-precision, real-time analysis—an area where the proposed diplexer excels due to its efficient field confinement and superior FBW characteristics.

Application of the proposed diplexer in sensing systems

The proposed low-pass/band-pass diplexer is not only a compact RF structure but also functions as a highly sensitive microwave sensor for detecting dielectric variations in pharmaceutical syrups. Specifically, it is designed

References	Operating frequency (GHz)	Configuration	FBW (%)	$\|S_{21}\|$(dB)	$\|S_{11}\|$(dB)	Size (mm × mm)
[27]	BP : 5.38, 6.68	BP/BP	BP : 3.35, 3	BP : 1.5, 1.2	> 10	92.8 × 33.1
	BP : 5.98, 7.38		BP : 2.84, 2.48	BP : 1.4, 1.5		
[28]	BP : 2.12, 3.9	BP/BP	BP : 5.66, 6.15	BP : 2.27, 2	BP : 17, 20.5	19.5 × 21.1
	BP : 2.45, 4.48		BP : 6.12, 5.13	BP : 2.88, 2.71	BP : 22, 21	
[29]	LP : 0.55	BP/LP	LP : 40	LP : 0.25	LP : 13	48 × 46
	BP : 2.4		BP : 5	BP : 1.2	BP : 12.5	
[30]	LP : 1.65	BP/LP	NA	LP : 0.2	LP : 15	24.9 × 33.9
	BP : 3, 6.2			BP : 0.8, 1.2	BP : 38, 12	
[31]	BP : 2.84	BP/BP	BP : 1.41	BP : 0.7	BP : 21.2	24 × 18
	BP : 4.08		BP : 2.2	BP : 0.9	BP : 17	
[32]	BP : 1.66	BP/BP	NA	BP : 3.2	BP : 16	32 × 26
	BP : 2.52			BP : 2.88	BP : 21	
This work	LP : 0.59	BP/LP	LP : 48.4	LP : 0.087	LP : 32.7	13.1 × 15.84
	BP : 1.48, 2.15		BP : 17.45, 14.6	BP : 0.045, 0.056	BP : 22.1, 23.5	

Table 2. Performance comparison with previously reported diplexers.

to quantify the concentration of key sweetening agents—sucrose and sorbitol—commonly found in syrups such as Diphenhydramine, Guaifenesin, and Salbutamol formulations.

The sensing capability of the diplexer arises from its ability to detect shifts in the resonant (center) frequencies of its filters, which are sensitive to the effective dielectric constant (ε_r) of the MUT. When a pharmaceutical syrup sample is introduced into the sensing region—strategically placed between the filters—it perturbs the local electromagnetic field distribution, altering the effective permittivity seen by the resonators.

This shift in dielectric loading causes a measurable variation in the center frequency f_c of each passband. The fundamental relationship governing the resonance of a microstrip resonator loaded with a dielectric sample is given by[1,2]:

$$f_c = \frac{c_0}{2L\sqrt{\varepsilon_r}} \tag{7}$$

where c_0 is the speed of light in vacuum (3×10^8 m/s), L is the effective electrical length of the resonator, ε_r is the effective dielectric constant of the sample. As each pharmaceutical syrup contains a different concentration of sucrose, sorbitol, moisture, and other constituents, it exhibits a unique dielectric signature. These differences in ε_r translate into distinct shifts in f_c, allowing the sensor to distinguish between syrup types and determine the concentration of targeted analytes.

The proposed diplexer features three distinct passbands, enabling simultaneous multi-parameter sensing. The three distinct passbands were strategically utilized for the quantification of sucrose and sorbitol across three different pharmaceutical syrup formulations. The sample is inserted between the filters, ensuring localized interaction with the resonant fields and minimizing electromagnetic coupling between adjacent filter paths, which enhances the sensor's selectivity and accuracy. The variation in the center frequency Δf_c due to a change in the effective permittivity $\Delta\varepsilon_r$ is approximately linear for small perturbations and can be expressed as:

$$\Delta f_c = -\frac{1}{2}\frac{f_c}{\varepsilon_r}\Delta\varepsilon_r \tag{8}$$

Alternatively, a simplified empirical relationship often used in sensitivity analysis is[1,2]:

$$\Delta f_c = k.\Delta\varepsilon_r \tag{9}$$

where, k is a proportionality constant determined by the filter's geometry and operating frequency. Also, to determine the most sensitive region within the diplexer structure for sample placement, current density distribution simulations were performed using ADS software. The resulting current distribution profiles are illustrated in Fig. 8a–d. Figure 8a through 8c correspond to the structure's passband frequencies at 0.59 GHz, 1.48 GHz, and 2.15 GHz, respectively. At these frequencies, the current density distribution clearly indicates that the majority of the electromagnetic energy is concentrated at the output ports, confirming efficient signal transmission through the corresponding channels. In contrast, Fig. 8d represents the structure's behavior at 6.00 GHz, a stopband frequency, where the resonator network effectively suppresses current flow, demonstrating its filtering capability. The comparison of these distributions provides valuable insight into the field behavior across the diplexer's operational spectrum and assists in identifying regions of maximal field interaction for sensor application.

A particularly notable observation from these simulations is the consistently high current density in the region between the two filter sections, regardless of the excitation frequency. This region exhibits strong localized electromagnetic fields, indicating it as the most sensitive area within the structure. Consequently, this inter-filter region is identified as the ideal location for placing the pharmaceutical syrup sample. The strong field

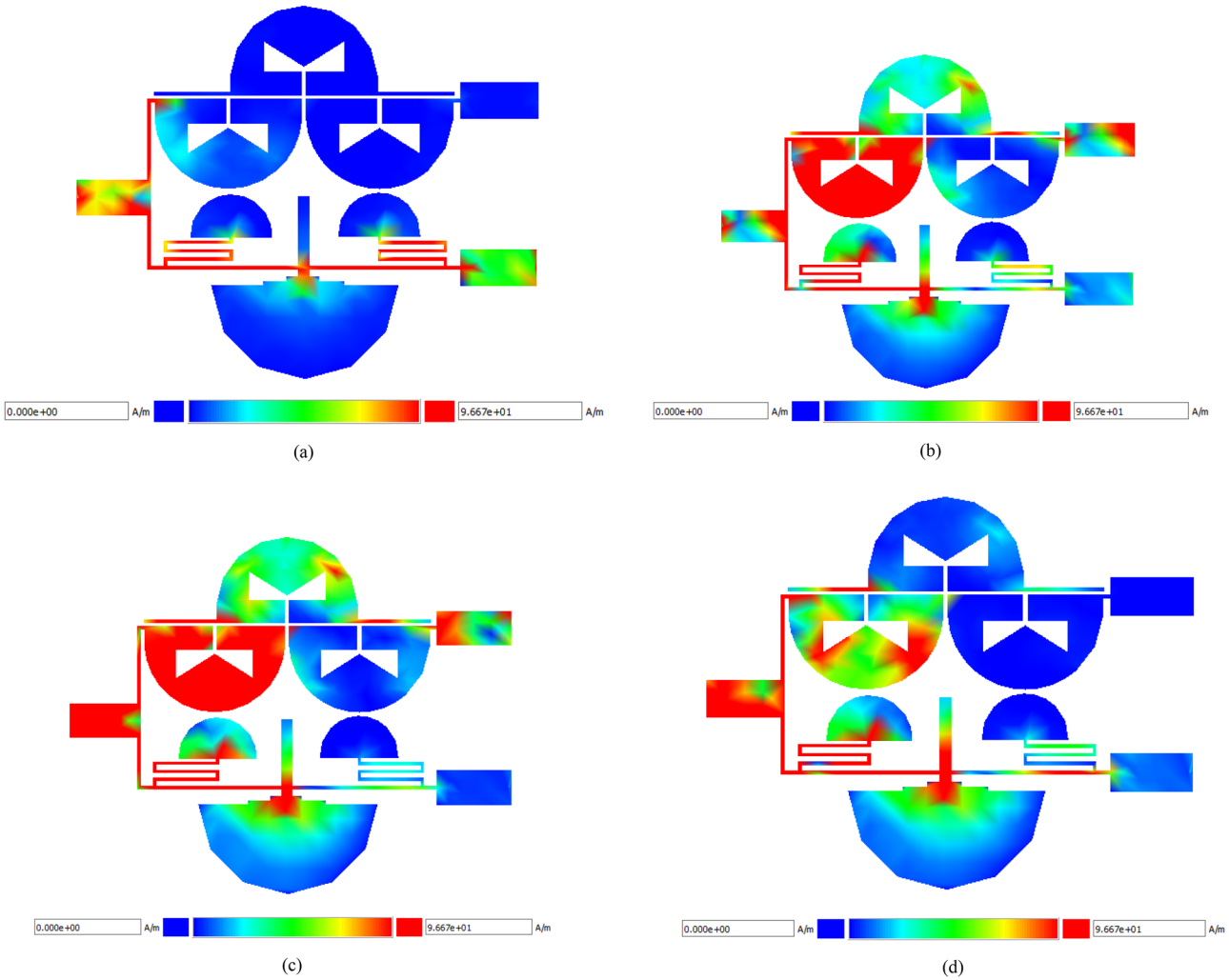

Fig. 8. Current density distribution across operating frequencies (**a**) 0.59 GHz—low-frequency passband, (**b**) 1.48 GHz—first mid-frequency passband, (**c**) 2.15 GHz—second-frequency passband, (**d**) 6.00 GHz—stopband frequency response.

interaction in this area ensures enhanced perturbation of the resonator response due to changes in the dielectric properties of the sample, thus maximizing the sensor's sensitivity and improving the accuracy of sucrose and sorbitol detection.

Furthermore, to enable accurate quantification, the sensor must be calibrated for each type of pharmaceutical syrup, as the base dielectric constant $\varepsilon_{r,0}$ varies by formulation. Calibration curves are generated by recording f_c across known concentrations of sucrose and sorbitol and correlating them with corresponding dielectric shifts. The sensitivity S of the sensor is defined as:

$$S = \frac{\Delta f_c}{\Delta c} \tag{10}$$

where Δc is the change in concentration (e.g., g/mL) of sucrose or sorbitol, and Δf_c is the associated shift in center frequency. This metric quantifies the sensor's responsiveness and is critical for evaluating its resolution and detection limits. Also, this methodology aligns with previous works in dielectric sensing where local sensitivity maxima are reported based on derivative behavior of non-linear calibration curves.

The integration of both LPF and BPF in the diplexer structure plays a pivotal role in enhancing the overall sensitivity of the microwave sensor. Each filter contributes differently to this enhancement based on its frequency-selective behavior and field confinement characteristics. Specifically, the LPF section provides high field concentration at lower frequencies, which is beneficial for detecting subtle changes in dielectric properties of materials with relatively high permittivity, such as sucrose-rich formulations. The LPF's roll-off region exhibits steep transitions, and the passband exhibits strong electromagnetic confinement, which amplifies small dielectric perturbations. This results in improved frequency resolution and hence higher sensitivity for low-frequency analytes.

On the other hand, the BPF section is tailored to operate at mid-to-high frequency ranges using M-notch resonators with superior Q-factor and tighter field localization. These resonators are more sensitive to small changes in effective permittivity due to their narrower bandwidth and stronger field confinement in a reduced sensing area. As a result, BPF paths are highly effective in detecting variations caused by analytes such as sorbitol that induce subtler shifts in dielectric constant.

By combining both filter types, the sensor leverages their complementary frequency sensitivities to achieve multi-band, multi-analyte detection. This configuration ensures that both coarse and fine dielectric shifts are captured, effectively broadening the dynamic range and maximizing overall sensitivity. Furthermore, the spatial separation of LPF and BPF paths minimizes mutual interference, allowing independent, high-precision sensing in each band.

Importance of sucrose and sorbitol quantification in pharmaceutical syrups

Accurate quantification of sucrose and sorbitol in oral pharmaceutical syrups is of paramount importance in both pharmaceutical manufacturing and clinical settings. These sweeteners are commonly used as excipients to enhance the palatability of oral liquid formulations, especially for pediatric and geriatric patients who may be sensitive to unpleasant tastes. However, beyond their role as flavoring agents, the concentration of these sugars directly influences the physicochemical stability, viscosity, osmolarity, and bioavailability of the active pharmaceutical ingredients (APIs)[33–36]. Excessive levels of sucrose can lead to issues such as dental caries, hyperglycemia, and metabolic imbalance, particularly in diabetic or sugar-sensitive individuals. Similarly, while sorbitol is often used as a sugar substitute due to its lower glycemic impact, it is also known to cause gastrointestinal distress—such as bloating, diarrhea, and abdominal pain—if consumed in high concentrations. Consequently, ensuring that the sucrose and sorbitol content remains within pharmaceutically acceptable limits is critical for ensuring safety, therapeutic efficacy, and regulatory compliance of oral syrup formulations. Traditional chemical analysis methods such as HPLC or enzymatic assays, while accurate, are time-consuming and often require extensive sample preparation. Thus, the development of microwave-based, non-invasive sensors—as proposed in this work—presents a compelling alternative for real-time and inline monitoring of these compounds during production and quality control processes[33–37].

Among the wide range of oral syrups available on the market, Diphenhydramine, Guaifenesin, and Salbutamol syrups are among the most widely used for managing respiratory conditions. Diphenhydramine is an antihistamine commonly prescribed for the relief of allergy symptoms such as sneezing, itching, and runny nose, and it also possesses sedative properties that make it useful as a nighttime cold remedy. Guaifenesin functions as an expectorant, facilitating the clearance of mucus from the airways in conditions such as bronchitis and the common cold. Salbutamol (also known as Albuterol) is a bronchodilator frequently used in the treatment of asthma and chronic obstructive pulmonary disease (COPD), helping to relax bronchial muscles and improve airflow. These syrups are often administered to vulnerable populations including children, the elderly, and patients with chronic respiratory illnesses—groups for whom dosage precision and formulation consistency are vital[33–40]. Given that these syrups are administered over repeated dosing schedules, accurate measurement of excipients such as sucrose and sorbitol become essential not only to ensure consistent therapeutic delivery but also to prevent long-term adverse effects due to cumulative sugar intake. Moreover, excipient variability can affect the rheological properties of the formulation, which in turn can influence dosing accuracy and patient adherence. Therefore, integrating precise, non-invasive sensing technologies into the quality control process of such syrups is highly beneficial and aligns with the pharmaceutical industry's growing emphasis on Quality by Design (QbD) and Process Analytical Technology (PAT) initiatives[33–40].

In typical pharmaceutical syrup formulations, the concentration of sucrose ranges from 3 to 6% w/v, serving not only as a sweetening agent but also as a preservative and viscosity enhancer. Sorbitol concentrations, when used, generally fall within the range of 1% to 3% w/v, depending on the desired sweetness level and the target patient population—especially in formulations intended for diabetic or sugar-sensitive patients, where it may partially or completely replace sucrose. In Diphenhydramine syrups, sucrose is typically used in higher concentrations to mask the bitter taste of the API, often nearing the upper limit of the acceptable range. In contrast, Guaifenesin syrups frequently use a combination of sucrose and sorbitol to strike a balance between sweetness and gastrointestinal tolerability. Salbutamol syrups, particularly pediatric versions, may incorporate sorbitol as the primary sweetener to reduce sugar content and improve tolerability. Deviations from the standard concentrations—whether intentional or due to production inconsistencies—can result in product recall, regulatory non-compliance, or patient safety concerns. Thus, a sensing system capable of distinguishing and quantifying subtle variations in the dielectric properties caused by different sucrose and sorbitol concentrations would provide a valuable quality control tool, ensuring batch-to-batch consistency and enhancing overall drug safety[37–44].

Testing and measurement

To evaluate the sensing performance of the proposed diplexer-based microwave sensor, experimental measurements were conducted using three widely used pharmaceutical syrups: Diphenhydramine, Guaifenesin, and Salbutamol. The primary objective was to detect and quantify the concentrations of sucrose and sorbitol present in these formulations. For each syrup type, three distinct commercial brands available on the Iranian pharmaceutical market were selected to account for variations in formulation among different manufacturers. Each sample was measured five times to ensure reproducibility and statistical reliability, resulting in a total of 45 independent measurements.

As depicted in Fig. 9a, all measurements were performed using an network analyzer, which offers high-precision S-parameter characterization across the desired frequency range. To maintain experimental consistency, all tests were carried out under controlled environmental conditions, with constant ambient temperature and

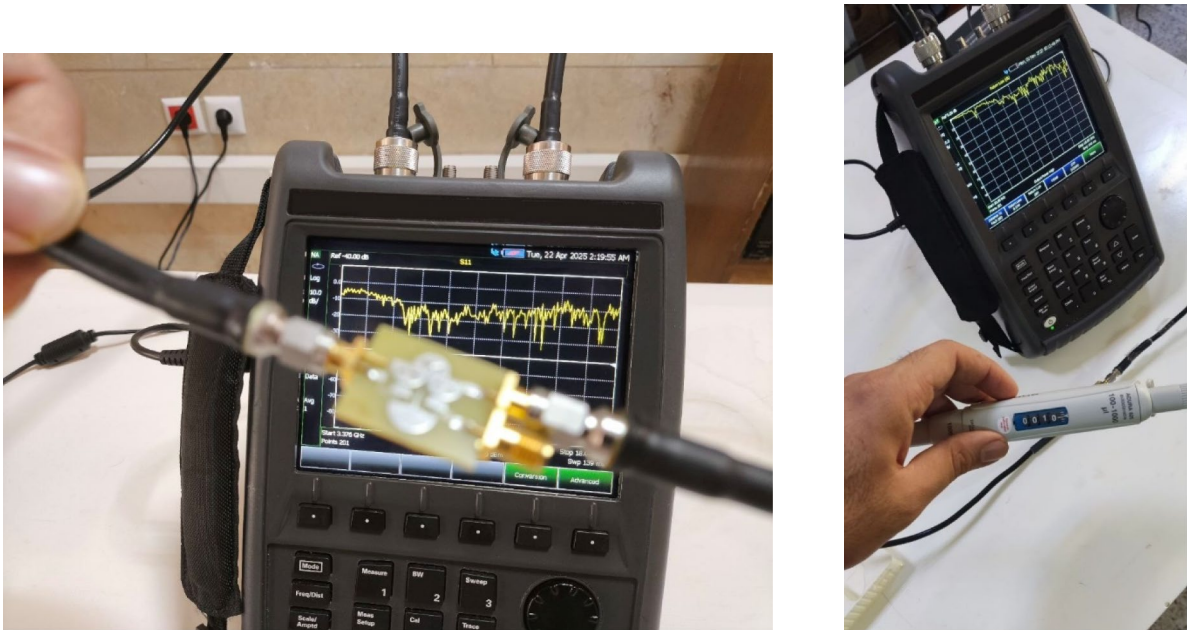

(a) (b)

Fig. 9. Experimental setup for sensor validation (**a**) measurement setup using network analyzer, (**b**) digital micropipette used for precise sample injection.

minimal external interference. A digital micropipette was employed to introduce precisely measured volumes of syrup samples into the sensor's test region, as illustrated in Fig. 9b. Moreover, efforts were made to conduct the measurements in an electromagnetically isolated environment to minimize noise and external coupling effects, thereby enhancing the accuracy and reliability of the experimental data.

Figures 10a–c present the measurement results and corresponding fitted curves illustrating the relationship between central frequency shifts and sucrose/sorbitol concentrations in three pharmaceutical syrups: Diphenhydramine, Guaifenesin, and Salbutamol, respectively. Given the inherently nonlinear behavior observed in the experimental data, curve fitting techniques were applied to model the trends and facilitate future estimation of sweetener concentrations based on measured frequency shifts. This approach enhances the sensor's practical utility by enabling predictive concentration analysis from real-time frequency measurements.

Each measurement was conducted using one of the three center frequencies associated with the diplexer structure. The first center frequency, corresponding to the LPF, was employed for analyzing Diphenhydramine syrup (Fig. 10a). The results demonstrate a nonlinear correlation: as the central frequency increases, the sucrose concentration also increases, while the sorbitol concentration exhibits an inverse trend. The second center frequency, associated with the first BPF, was used for Guaifenesin syrup (Fig. 10b). Among the three samples, this syrup exhibited the most complex and nonlinear response, particularly for sorbitol, making its behavior more challenging to predict with simple models. Finally, the third center frequency, related to the second BPF, was used to characterize Salbutamol syrup (Fig. 10c). In this case, the fitted curves—especially for sorbitol concentration—demonstrate a more linear and predictable trend, indicating a stronger correlation between dielectric properties and frequency shift.

These results confirm the sensor's sensitivity to dielectric variations caused by changes in sweetener concentrations and highlight its potential for quantitative, real-time analysis of pharmaceutical syrups across multiple formulations. It is important to note that the pharmaceutical syrups used in this study were commercially available standard formulations, commonly found in the consumer market. The objective was not to evaluate sugar-free or specially formulated syrups intended for diabetic patients or pregnant women, but rather to assess the sensor's performance under typical conditions reflective of standard pharmaceutical use.

Based on the experimental results presented in Fig. 10 and utilizing the sensitivity relationship defined in Eq. (10), the measurement sensitivity of the proposed sensor for each pharmaceutical syrup was calculated. The corresponding sensitivity values for sucrose and sorbitol across the different formulations are summarized in Table 3. These values provide a quantitative assessment of the sensor's responsiveness to variations in the dielectric properties of the tested syrups.

The calibration process of the proposed diplexer-based microwave sensor was meticulously conducted using three well-characterized pharmaceutical syrups as reference materials. These reference samples, verified with standard analytical methods, provided baseline frequency measurements under controlled conditions using a network analyzer. Following this, additional commercial syrup brands were tested to record frequency shifts corresponding to varying concentrations of sucrose and sorbitol. The data were analyzed through a curve-fitting process, resulting in a robust calibration curve as depicted in Fig. 10. This curve enables the real-time prediction

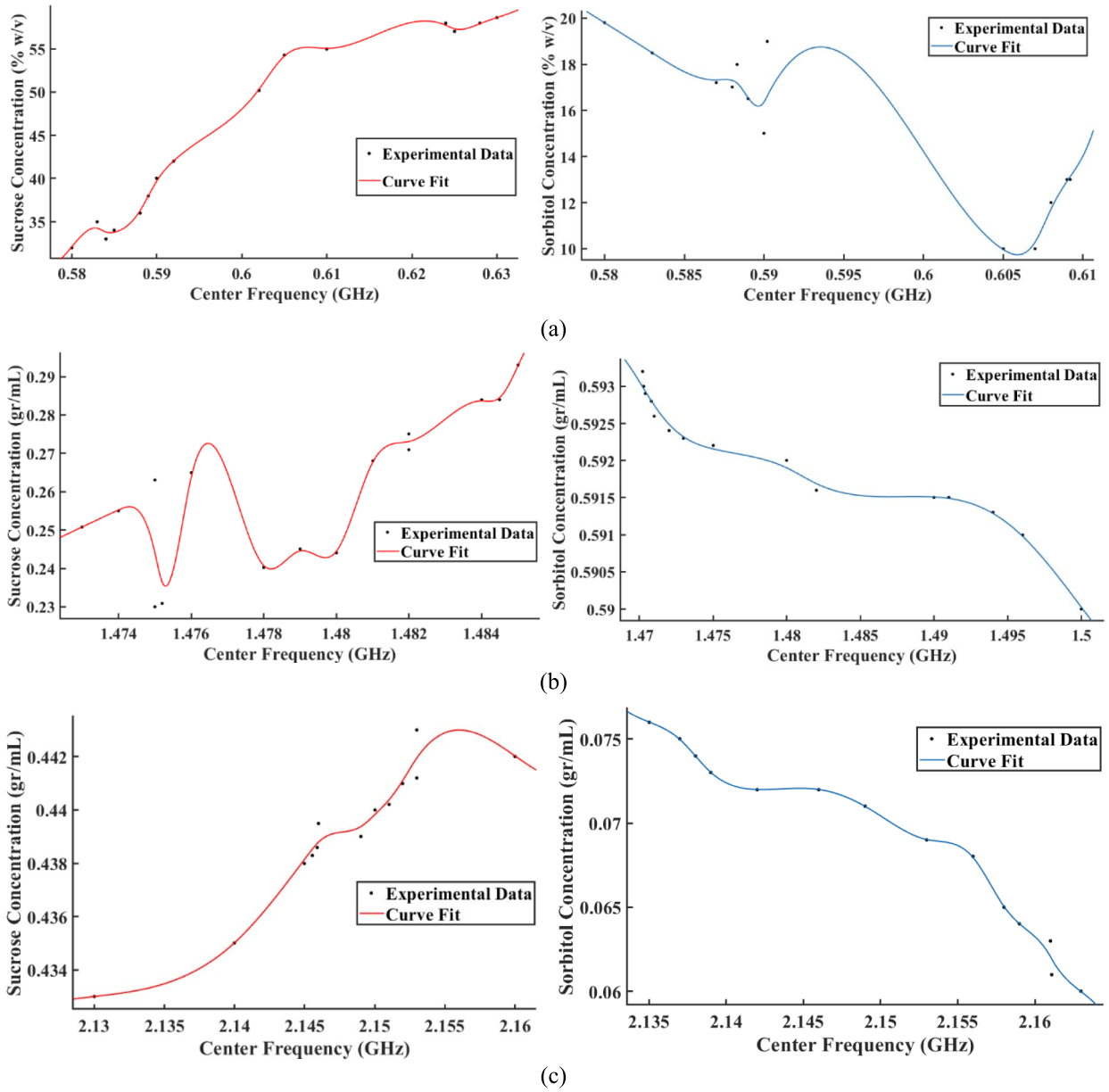

Fig. 10. Sweetener concentration vs. central frequency shift in pharmaceutical syrups (**a**) Diphenhydramine, (**b**) Guaifenesin, (**c**) Salbutamol—measurement results and fitted response curves for sucrose and sorbitol concentrations.

Type of syrup	Sucrose Sensitivity	Sorbitol Sensitivity	Sucrose DL	Sorbitol DL
Diphenhydramine	1879.69 ($\frac{\text{KHz}}{\%}$)	2979.59 ($\frac{\text{KHz}}{\%}$)	0.00184 ($\frac{\text{dB.\%}}{\text{KHz}}$)	0.00116 ($\frac{\text{dB.\%}}{\text{KHz}}$)
Guaifenesin	8000 ($\frac{\text{MHz}}{\text{gr/mL}}$)	9312.5 ($\frac{\text{MHz}}{\text{gr/mL}}$)	0.00043 ($\frac{\text{dB.gr}}{\text{MHz.mL}}$)	0.00037 ($\frac{\text{dB.gr}}{\text{MHz.mL}}$)
Salbutamol	3000 ($\frac{\text{MHz}}{\text{gr/mL}}$)	2800 ($\frac{\text{MHz}}{\text{gr/mL}}$)	0.00115 ($\frac{\text{dB. gr}}{\text{MHz.mL}}$)	0.00123 ($\frac{\text{dB.gr}}{\text{MHz.mL}}$)

Table 3. Sensor sensitivity and DL for sucrose and sorbitol detection in pharmaceutical syrups (Sensitivity values represent the local maximum slope of the fitted calibration curves derived from measured frequency shifts in response to analyte concentration. These values reflect the steepest response region per analyte and do not indicate the total frequency shift across the full concentration range.)

of analyte concentrations based on observed frequency deviations. Importantly, all tests were performed under identical conditions, and the sensor's precision ensures that even if its absolute accuracy is slightly variable, the reliability of concentration predictions remains unaffected. The evaluation is fundamentally based on the precision of frequency change, making the sensor highly practical for non-invasive, real-time pharmaceutical monitoring.

Figure 11 illustrates the step-by-step process for the calibration and measurement of sucrose and sorbitol concentrations using the proposed diplexer-based microwave sensor. The procedure begins with the preparation of reference materials with known concentrations of sucrose and sorbitol. These reference samples are tested using a Network Analyzer to measure their central resonant frequencies, which are fundamental indicators of their dielectric properties. The choice of these center frequencies is grounded in a combination of physical reasoning and simulation-based analysis. Initially, the expected permittivity changes associated with sucrose and sorbitol were theoretically evaluated, guiding the design of the resonator structures to isolate specific frequency bands. This theoretical foundation was further validated through electromagnetic simulations to optimize the sensor's dual-path architecture for distinct low-pass and band-pass filtering. The process continued with the testing of various commercial syrup brands, where the sensor's frequency shifts (Δf) were recorded and mapped through curve fitting to establish a robust calibration curve, as illustrated in Fig. 10. This curve enables real-time prediction of analyte concentrations in unknown samples by directly correlating observed frequency deviations to specific concentration levels, ensuring high precision and reliability in pharmaceutical analysis.

In other words, the allocation of the center frequencies for sucrose and sorbitol detection in the proposed diplexer-based microwave sensor was methodically determined using reference materials with known analyte concentrations. These reference samples exhibited unique and stable resonant frequencies when tested with the sensor, serving as the baseline for all subsequent measurements. The process involved recording frequency shifts (Δf) relative to these reference frequencies, enabling precise mapping of concentration changes without relying on trial-and-error adjustments. A robust calibration curve, as depicted in Fig. 10, was established to correlate frequency deviations with analyte concentrations, allowing for accurate, real-time predictions in pharmaceutical syrups.

Measurement repeatability refers to the sensor's ability to consistently produce the same output under identical testing conditions across multiple trials. High repeatability, indicated by a low standard deviation, reflects the sensor's precision and stability. In combination with measurement uncertainty, repeatability plays a crucial role in evaluating the reliability and robustness of the sensor for long-term or repeated use[45].

The measurement uncertainty arises from various contributing factors, including sample preparation inconsistencies, environmental fluctuations (e.g., temperature and humidity), measurement noise, and fabrication tolerances. To accurately quantify this uncertainty, a series of repeatability tests and environmental variation analyses were performed. Furthermore, Monte Carlo simulations were employed to statistically model the collective impact of these error sources. The standard deviation (SD) of the frequency shifts across repeated measurements was determined to be less than 153 kHz, signifying excellent repeatability. Using the standard method for estimating uncertainty, the overall measurement uncertainty was calculated as:

$$U = 2 \times SD = 306\,\mathrm{KHz} \tag{11}$$

This level of uncertainty confirms the sensor's reliability under practical conditions and highlights its potential for use in real-world pharmaceutical quality control. Also, to experimentally assess repeatability, each pharmaceutical syrup sample was tested five times. In each trial, a precise volume of 0.1 mL of the sample was dispensed onto the sensor's active surface using a digital micropipette. After recording the S-parameter data, the sensor surface was thoroughly cleaned and dried to eliminate any residue before repeating the measurement. This protocol ensured consistent environmental and procedural conditions, allowing for an accurate assessment of the sensor's measurement stability.

The DL is a key metric in evaluating sensor performance, as it defines the minimum detectable amount of a target analyte—in this case, sucrose and sorbitol—that can be distinguished from background noise with high confidence. A sensor's ability to detect such low concentrations is fundamental to its practical utility, especially in pharmaceutical applications where minute compositional changes can affect product quality. The DL is closely tied to the signal-to-noise ratio (SNR): the sensor must produce a measurable and statistically significant signal response in the presence of the analyte, while minimizing interference from inherent noise or environmental fluctuations. To quantify this capability, a statistical approach is employed, leveraging a commonly used expression in analytical science[46]:

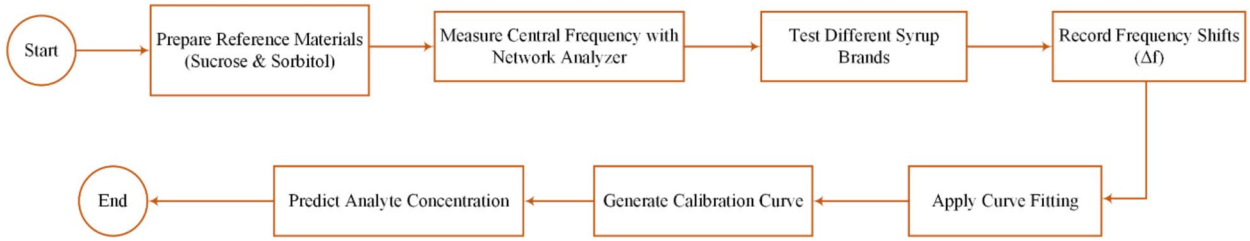

Fig. 11. Measurement process flowchart.

$$DL = \frac{3.3 \times \sigma_{noise}}{S} \tag{12}$$

In this context, σ_{noise} denotes the standard deviation of background signal fluctuations, while S represents the sensor's sensitivity to changes in the analyte's dielectric properties. Given that this study involves the detection of two analytes—sucrose and sorbitol—across three different pharmaceutical syrups, each with distinct sensitivity values, the DL was computed individually for each case. The resulting values are summarized in Table 3.

The data presented in Table 3 reflect the sensor's capability to detect minute dielectric changes in each syrup type, corresponding to subtle variations in sucrose and sorbitol concentrations. The use of the 3.3 coefficient in the DL calculation ensures a confidence level of approximately 99%, thereby minimizing the likelihood of misinterpreting background noise as a true signal. This high level of statistical reliability reinforces the accuracy of the sensor's output under practical conditions. Overall, the exceptionally low detection limits achieved in this study underscore the sensor's high sensitivity and reliability, establishing it as a robust platform for precise, non-invasive, and real-time monitoring of pharmaceutical syrups in quality control and formulation validation processes.

All pharmaceutical syrup samples were precisely administered using a calibrated digital micropipette, ensuring a consistent volume of 0.1 mL per trial and maintaining uniformity across all measurement conditions. This volume was selected to ensure adequate interaction with the sensor surface while remaining well above the sensor's minimum detectable threshold. Following deposition, sufficient time was allowed for the sample to naturally settle and distribute across the sensor's active region, promoting homogeneous dielectric loading. Achieving a uniform coating was essential to minimize spatial inconsistencies that could otherwise affect measurement repeatability and accuracy.

So, the choice of sample volume not only ensured consistent detection of minor changes in dielectric properties but also contributed to enhanced measurement stability by reducing the influence of localized variations in sample positioning. All measurements were conducted under strictly controlled environmental conditions, thereby ensuring a high degree of repeatability and reproducibility. An important aspect of the experimental setup was the hydrophobic nature of the sensor surface, characterized by a contact angle exceeding 45 degrees. This surface property played a critical role in maintaining sample integrity by preventing uncontrolled spreading of the syrup. As a result, each sample remained confined to the designated sensing region, preserving the consistency of the interaction area and enhancing measurement reliability. The hydrophobic behavior of the microstrip diplexer thus provided a form of passive dielectric isolation, ensuring precise localization of the analyte and contributing to the overall robustness of the sensing system.

The experimental results validate that the proposed diplexer-based microwave sensor achieves an observed peak sensitivity of 9312.5 MHz/(g mL^{-1}) specifically for Guaifenesin, marking it as the highest sensitivity detected across all tested pharmaceutical syrups. This exceptional level of sensitivity was consistently measured under identical experimental conditions, as presented in Fig. 10 and Table 3, confirming its superior dielectric response. It should be noted that, the observed variations in sensitivity among the tested pharmaceutical syrups—Diphenhydramine, Guaifenesin, and Salbutamol—can be attributed to the distinct dielectric properties and molecular compositions inherent to each formulation. These differences influence the interaction between the sensor's electromagnetic fields and the syrup constituents, thereby affecting the sensor's sensitivity.

The sensitivity values reported in Table 3, including the maximum of 9312.5 MHz/(g mL^{-1}), were calculated based on the slope of the fitted nonlinear calibration curve relating the resonant frequency shift (Δf) to the concentration of the analyte (sucrose or sorbitol) in a given syrup formulation. Specifically, the value of 9312.5 MHz/(g mL^{-1}) corresponds to the maximum local slope (first derivative) of the fitted response curve for sorbitol concentration in Guaifenesin syrup.

Guaifenesin syrup

Guaifenesin syrup demonstrated the highest sensitivity among the tested formulations, with a peak sensitivity of 9312.5 MHz/(g mL^{-1}). This exceptional performance is primarily linked to its molecular composition. Guaifenesin ($C_{10}H_{14}O_4$) contains both ether and hydroxyl functional groups, which are known for their strong polarizability and high dielectric constant, enhancing their interaction with electromagnetic fields. Additionally, common excipients such as glycerin and citric acid, both highly polar, further elevate the dielectric response of the syrup. Glycerin's hydroxyl groups, in particular, contribute to high permittivity, enabling stronger coupling with the sensor's resonant fields and resulting in significant shifts in resonant frequency during the detection process[47–50].

Diphenhydramine syrup

Diphenhydramine syrup exhibited a sensitivity of 2979.59 ($\frac{KHz}{\%}$), very lower compared to guaifenesin. This can be explained by its active ingredient, Diphenhydramine HCl ($C_{17}H_{21}NO$), which, while possessing polar amine groups, exhibits a lower overall dielectric constant than guaifenesin. Additionally, the syrup contains propylene glycol as a stabilizer, which, despite its hygroscopic nature, has a moderate dielectric response compared to glycerin. Consequently, the interaction with the sensor's electromagnetic fields is less pronounced, leading to a relatively lower sensitivity[47–50].

Salbutamol syrup

Salbutamol syrup recorded a sensitivity of 2979.59 ($\frac{KHz}{\%}$), slightly lower compared to diphenhydramine. The active ingredient, Salbutamol Sulfate ($C_{13}H_{21}NO_3{\cdot}H_2SO_4$), is moderately polar, and its excipients include sorbitol and sodium benzoate. Sorbitol, a sugar alcohol, contains multiple hydroxyl groups that elevate its dielectric constant, improving interaction with the sensor's electromagnetic waves. This results in a signal response close

References	Size (mm × mm)	Sensitivity	DL ($\frac{dB.\varepsilon_r}{MHz}$) or equivalent)	Circuit structure	Sensing application
[15]	40 × 25	0.85% are achieved at a maximum permittivity of 78.3	NA	band-stop filter	General dielectric constant sensing
[16]	24.7 × 30	7200 ($\frac{MHz}{gr/mL}$)	NA	coupler	Blood glucose concentration detection
[51]	70 × 70	1.87 ($\frac{MHz}{\varepsilon_r}$)	1.94	antenna	Purity evaluation of edible oils
[52]	42.3 × 12.1 × 0.787	2.44 ($\frac{MHz}{\varepsilon_r}$)	1.48	band-pass filter	Oil–water mixture concentration monitoring
[53]	40 × 40	0.12 ($\frac{MHz}{\varepsilon_r}$)	30.25	band-stop filter	Water content detection in oil samples
[54]	30 × 25 × 1.6	0.04 ($\frac{MHz}{\varepsilon_r}$)	NA	band-stop filter	Liquid material composition analysis
[55]	10.3 × 10.5	887 ($\frac{MHz}{\varepsilon_r}$)	0.0037	Power divider	Purity evaluation of edible oils
[56]	9.27 × 16.24	188 ($\frac{MHz}{\varepsilon_r}$)	0.0183	triplexer	Honey quality detection
[57]	30 × 20	24 ($\frac{dB}{gr/dL}$)	3–5 mg/dL	Meta-surface	Blood glucose measurement
This work	13.1 × 15.84	9312.5 ($\frac{MHz}{gr/mL}$) (highest)	0.00037 ($\frac{dB.gr}{MHz.mL}$) (lowest)	diplexer	Multi-analyte detection in pharmaceutical syrups

Table 4. Evaluation of the sensor's performance compared to previously reported designs.

to that of diphenhydramine, but still inferior to that of guaifenesin due to differences in molecular structure and polarizability[47–50].

In summary, the distinct molecular configurations and dielectric characteristics of the active pharmaceutical ingredients and excipients play a critical role in modulating the electromagnetic field interactions within the proposed microwave sensor. Among the tested formulations, Guaifenesin exhibits the highest sensitivity, attributed to its pronounced molecular polarity and the inclusion of highly polar excipients such as glycerin, which collectively enhance field confinement and electromagnetic coupling. In contrast, Diphenhydramine and Salbutamol demonstrate comparatively lower sensitivity, a reflection of their reduced polarizability and correspondingly diminished electromagnetic interactions. The strategic architectural design of the sensor, leveraging M-notch and semicircular resonators, is optimized to capitalize on these dielectric differences. By precisely localizing the electromagnetic fields to target-specific permittivity shifts, the sensor achieves exceptional sensitivity and resolution, facilitating accurate and real-time quantification of sucrose and sorbitol concentrations in pharmaceutical syrups. This targeted field manipulation underscores the sensor's capability for high-resolution detection across varying chemical compositions, establishing it as an advanced platform for non-invasive pharmaceutical analysis. It is noteworthy that the sensitivity spectrum for the various pharmaceutical formulations extends from 1879.69 kHz/% for Diphenhydramine to 9312.5 MHz/(g mL^{-1}) for Guaifenesin, underscoring the sensor's robust capability to achieve high-resolution detection across diverse syrup compositions.

Table 4 provides a comparative analysis of the proposed diplexer-based microwave sensor alongside a series of previously reported designs in terms of device size, sensitivity, DL, circuit structure, and sensing application. The analysis highlights the key technological advancements and innovative features introduced by the proposed sensor, positioning it as a leading solution in microwave-based pharmaceutical sensing.

In examining the table, it is evident that the proposed sensor achieves a uniquely compact footprint compared to many conventional designs. While certain designs, such as the one presented in[55], may have slightly smaller dimensions, this reduction in size comes at the cost of significantly poorer sensitivity and limited detection capability. The power divider configuration in[55] is specifically tailored for single-parameter evaluation, which limits its applicability for complex multi-analyte detection. In contrast, the proposed sensor not only maintains a highly optimized size but also introduces multi-analyte detection for sucrose and sorbitol in pharmaceutical syrups—an innovation not present in any of the referenced works. Moreover, while designs like Ref.[53] feature relatively compact band-stop filter structures, their sensitivity and detection accuracy are notably weaker. These designs are mainly focused on single-material detection, such as water content in oil, and are not equipped for the precision needed in pharmaceutical analysis. The proposed diplexer, on the other hand, effectively leverages its dual-path low-pass and band-pass architecture to achieve enhanced electromagnetic field confinement, resulting in high-resolution detection of two distinct analytes simultaneously. When comparing with larger designs, such as those reported in[15] and[51], the differences become even more pronounced. These designs occupy substantially more physical space yet fail to deliver the multi-band sensitivity and low detection limits required for fine concentration analysis in liquid solutions. The antenna structure in[51], for example, is bulky and optimized for general dielectric sensing, but its circuit complexity and limited detection resolution make it impractical for pharmaceutical syrup analysis. In contrast, the proposed sensor accomplishes superior sensitivity and dual-analyte detection in a far smaller and more efficient structure. Similarly, Ref.[16] presents a coupler design aimed at blood glucose detection. While it achieves reasonable sensitivity, its single-path configuration restricts it to monitoring only one analyte at a time. The proposed diplexer overcomes this limitation through its dual-path mechanism, enabling non-invasive, real-time monitoring of both sucrose and sorbitol without interference—an advancement that considerably enhances its applicability for pharmaceutical quality control.

The designs in[52] and[54] focus on oil–water mixture analysis and liquid material composition, respectively. While effective for specific industrial applications, their circuit complexity and bulkier architectures limit their scalability and integration into compact sensing platforms. Furthermore, these designs lack the multi-analyte capabilities of the proposed diplexer, which is specifically engineered to isolate distinct frequency bands for each target analyte. This design choice not only improves detection accuracy but also streamlines the analysis process in pharmaceutical applications. Furthermore, the sensing architectures described in[56] and[57] exhibit significantly lower sensitivity and higher detection limits compared to the proposed diplexer-based microwave sensor.

In summary, the proposed diplexer-based microwave sensor excels in four critical areas:

1. Compact Design: Achieves miniaturization without sacrificing performance, unlike bulkier conventional designs.
2. High Sensitivity and Low DL: Demonstrates superior electromagnetic field confinement for fine concentration detection.
3. Multi-Analyte Capability: Introduces simultaneous detection of sucrose and sorbitol, setting it apart from single-analyte sensors.
4. Simplified Circuit Structure: Utilizes a planar design with standard FR4 substrate, reducing fabrication costs and complexity.

These innovations mark the proposed design as a pioneering solution in non-invasive, real-time monitoring of pharmaceutical syrups, offering a combination of miniaturization, sensitivity, and multi-analyte functionality that is unmatched by current technologies.

The proposed diplexer-based microwave sensor is inherently designed for non-invasive pharmaceutical analysis due to its planar microstrip structure and dual-path configuration. Unlike invasive chemical methods that often require strict laboratory conditions, controlled temperatures, and extensive sample preparation, this sensor operates effectively in real-time with minimal environmental dependency. Chemical assays are also frequently destructive and irreversible, whereas the proposed sensor is completely non-destructive, non-harmful, and can be used repeatedly for millions of cycles without loss of performance. Furthermore, it eliminates risks associated with exposure to harmful chemicals, ensuring safety for both the device and the operator.

From a selectivity perspective, the proposed diplexer-based microwave sensor is engineered with a dual-path architecture consisting of low-pass and band-pass filters, each strategically designed to resonate at distinct frequency bands. This configuration allows for independent and interference-free quantification of sucrose and sorbitol even when both analytes are present in the same syrup matrix. The low-pass path is dedicated to capturing the dielectric response of sucrose, while the band-pass path is optimized for sorbitol detection. This strategic separation is reinforced by M-notch and semicircular resonators, which confine electromagnetic fields to their respective paths, preventing signal overlap and enhancing sensitivity. Additionally, the wide bandwidth available in each path enables versatile testing and supports multi-parameter analysis (S21, S11), allowing for cross-verification of sensor performance. This redundancy ensures that if one path experiences signal degradation, the other remains fully functional, reinforcing reliability. These design optimizations collectively establish the sensor's superior selectivity, making it an innovative solution for non-invasive, high-resolution monitoring of sucrose and sorbitol concentrations in pharmaceutical syrups.

Furthermore, the lumped-element LC circuit model presented in the design section further reinforces this capability by accurately predicting discrete frequency shifts for each analyte. This precise modeling enables sharp spectral isolation, which is essential for non-invasive, real-time quality control in pharmaceutical applications.

Conclusion

In this study, a novel diplexer-based microwave sensor was successfully designed, implemented, and validated for the non-invasive detection and quantification of sucrose and sorbitol concentrations in pharmaceutical syrups. The proposed sensor features a compact footprint of 13.1 mm × 15.84 mm and leverages a hybrid configuration of semicircular and M-notch-shaped resonators to enhance electromagnetic performance and frequency selectivity. The diplexer integrates low-pass and band-pass filters, producing three distinct operational bands, each employed to characterize a specific pharmaceutical syrup—Diphenhydramine, Guaifenesin, and Salbutamol. Experimental results demonstrated outstanding performance, with a maximum sensitivity of 9312.5 MHz/(g mL^{-1}) and a minimum DL of 0.00037 (dB g)/(MHz mL). Furthermore, the sensor exhibited a standard deviation of only 153 kHz across repeated measurements, confirming its high repeatability and stability. The sensor was fabricated on a standard FR4 substrate, and the measured and simulated results showed strong agreement, validating the accuracy of the design and modeling approach. With its high sensitivity, excellent measurement precision, and miniaturized structure, the sensor provides a cost-effective, reliable, and scalable solution for real-time monitoring of sweetener content in pharmaceutical formulations. Its robust performance and non-invasive nature make it highly suitable for both laboratory-based quality control and on-site diagnostic applications in the pharmaceutical industry.

Data availability

The datasets used and/or analysed during the current study available from the corresponding author on reasonable request.

Received: 28 March 2025; Accepted: 18 September 2025
Published online: 24 October 2025

References

1. Pozar, D. M. *Microwave Engineering: Theory and Techniques* (Wiley, 2021).
2. Hong, J. S. G. & Lancaster, M. J. *Microstrip Filters for RF/Microwave Applications* (Wiley, 2004).
3. Zonouri, S. A. & Hayati, M. A compact Gysel power divider with ultra-wide rejection band and high fractional bandwidth. *Int. J. RF Microwave Comput. Aided Eng.* **31**(6), e22643 (2021).
4. Zonouri, S. A. & Hayati, M. A compact ultra-wideband Wilkinson power divider based on trapezoidal and triangular-shaped resonators with harmonics suppression. *Microelectron. J.* **89**, 23–29 (2019).
5. Duan, S., Zhang, J. & Liu, M. Design of an ultra-small Wilkinson power divider using two-part resonators for S-band applications. *Multiscale Multidiscip. Model. Exp. Design* **6**(4), 643–655 (2023).
6. Zonouri, S. A., Hayati, M. & Bahrambeigi, M. Design of dual-band Wilkinson power divider based on novel stubs using PSO algorithm. *Int. J. Microw. Wirel. Technol.* **15**(9), 1495–1506 (2023).
7. Wan, X. et al. Compact switchable microstrip lowpass filter using cross-shaped resonator with sextuple states. *Microelectron. J.* **157**, 106565 (2025).
8. Liu, J., & Zhang, P. An ultra-small wideband diplexer with triangular-shaped and rectangular-shaped resonators for mobile base stations. *Electr. Eng.* 1–18 (2024).
9. Hussein, H. A., Mezaal, Y. S. & Alameri, B. M. Miniaturized microstrip diplexer based on fr4 substrate for wireless communications. *Elektronika Ir Elektrotechnika* **27**(5), 34–40 (2021).
10. Hsu, H. W. & Tu, W. H. Microwave microstrip six-channel triplexer and eight-channel quadruplexer. *IEEE Trans. Compon. Packag. Manuf. Technol.* **7**(7), 1136–1143 (2017).
11. Long, Z., Zhang, B., Liu, G., Wu, Z., & Yan, Q. A compact branch-line coupler with harmonic suppression using novel circular-shaped resonators for medical imaging systems. *Multiscale Multidiscip. Model. Exp. Design* 1–18 (2024).
12. Ahmed, F. H., Saad, R. & Khamas, S. K. A novel compact broadband quasi-twisted branch line coupler based on a double-layered microstrip line. *Micromachines* **15**(1), 142 (2024).
13. Zarghami, S., Zonouri, S. A., Bashi, S. M., Hatami, A. & Shah-Ebrahimi, S. M. A high-accuracy blood glucose detection sensor using tunable bandpass filter and MLP and RBF artificial neural network algorithms. *IEEE Sens. J.* **24**, 7778 (2024).
14. Li, W. et al. Simultaneous measurement of blade tip clearance and blade tip timing with microwave sensor. *IEEE Trans. Instrum. Meas.* **73**, 1–12 (2024).
15. Nikkhah, N., Keshavarz, R., Abolhasan, M., Lipman, J. & Shariati, N. Highly sensitive differential microwave sensor using enhanced spiral resonators for precision permittivity measurement. *IEEE Sens. J.* **24**, 14177 (2024).
16. Mohammadi, P., Mohammadi, A., Demir, S. & Kara, A. Compact size, and highly sensitive, microwave sensor for non-invasive measurement of blood glucose level. *IEEE Sens. J.* **21**(14), 16033–16042 (2021).
17. Rabbani, M. G. et al. Dumbbell shaped structure loaded modified circular ring resonator based perfect metamaterial absorber for S, X and Ku band microwave sensing applications. *Sci. Rep.* **14**(1), 5588 (2024).
18. Islam, M. R. et al. Quad-band split ring resonator-based sensor for microwave sensing application. *Sci. Rep.* **15**(1), 6888 (2025).
19. Al-Behadili, A. A., Mocanu, I. A., Petrescu, T. M. & Elwi, T. A. Differential microstrip sensor for complex permittivity characterization of organic fluid mixtures. *Sensors* **21**(23), 7865 (2021).
20. Yue, W. et al. Advancements in passive wireless sensing systems in monitoring harsh environment and healthcare applications. *Nano-Micro Lett.* **17**(1), 1–48 (2025).
21. Mezaal, Y. S., Ghazi, H. S. & Khaleel, M. H. Compact diplexer based on SIR feeders, T-shaped resonators, and UIR components for mobile wireless systems. *J. Electromagn. Waves Appl.* **39**, 1–16 (2025).
22. Khani, S., Roshani, S., Roshani, S. & Fouladian, M. Design and fabrication of an ultra small quadband diplexer integrated with a diplexed power amplifier for mid band 5G applications. *Sci. Rep.* **15**(1), 5087 (2025).
23. Dong, H. A small-size ultra-wide Wilkinson power divider based on a new ring-shaped resonator using the PSO algorithm. *J. Appl. Sci. Eng.* **27**(6), 2593–2603 (2024).
24. Luo, H., Song, Q. & Lai, S. A miniaturized branch-line coupler using new cleaver-shaped resonators with high FBW. *Forsch. Ingenieurwes.* **89**(1), 6 (2025).
25. Aljeboori, Z. W. J. & Malekshahi, M. R. ACOA-optimized microstrip gysel power divider with semi-radial-shaped resonators for broadband applications. *Multiscale Multidiscip. Model. Exp. Design* **7**(6), 5203–5216 (2024).
26. Al-Dwairi, M. O. A planar UWB semicircular-shaped monopole antenna with quadruple band notch for WiMAX, ARN, WLAN, and X-band. *Int. J. Electr. Comput. Eng. (2088–8708)* **10**(1), 908 (2020).
27. Wei, F., Liu, W. S., Wang, J. X. & Zhao, X. B. Design of a novel balanced-to-balanced dual-band diplexing power divider. *IEEE Trans. Circuits Syst. II Express Briefs* **70**(2), 516–520 (2022).
28. Gorur, A. K. et al. A high isolation quad-channel microstrip diplexer based on codirectional split ring resonators. *Microw. Opt. Technol. Lett.* **64**(8), 1382–1386 (2022).
29. Perez-Wences, C. et al. Compact microstrip lowpass-bandpass diplexer using radial stubs. *Microw. Opt. Technol. Lett.* **61**(2), 485–489 (2019).
30. Bavandpour, S. K., Roshani, S., Pirasteh, A., Roshani, S. & Seyedi, H. A compact lowpass-dual bandpass diplexer with high output ports isolation. *AEU-Int. J. Electron. Commun.* **135**, 153748 (2021).
31. Al-Majdi, K. & Mezaal, Y. S. New miniature narrow band microstrip diplexer for recent wireless communications. *Electronics* **12**(3), 716 (2023).
32. Mezaal, Y. S., Khaleel, S. K., Alameri, B. M., Al-Majdi, K. & Al-Hilali, A. A. Miniaturized microstrip dual-channel diplexer based on modified meander line resonators for wireless and computer communication technologies. *Technologies* **12**(5), 57 (2024).
33. Allen, L. & Ansel, H. C. *Ansel's Pharmaceutical Dosage Forms and Drug Delivery Systems* (Lippincott Williams & Wilkins, 2013).
34. Aulton, M. E. & Taylor, K. (eds) *Aulton's Pharmaceutics: The Design and Manufacture of Medicines* (Elsevier Health Sciences, 2013).
35. Shargel, L., Andrew, B. C., & Wu-Pong, S. Applied biopharmaceutics & pharmacokinetics (2005).
36. Phannarangsee, Y. et al. Sorbitol production from mixtures of molasses and sugarcane bagasse hydrolysate using the thermally adapted *Zymomonas mobilis* ZM AD41. *Sci. Rep.* **14**(1), 5563 (2024).
37. Acharya, P. et al. A review on analytical methods for determination of guaifenesin alone and in combination with other drugs in pharmaceutical formulations. *Saudi J. Med. Pharm. Sci* **3**, 148–159 (2017).
38. Lutomski, D. M., Gora, M. L., Wright, S. M., & Martin, J. E. Sorbitol content of selected oral liquids (1993).
39. Martindale, W. & Sweetman, S. C. *Martindale: The Complete drug Reference* (Pharmaceutical Press, 1999).
40. Rowe, R. C., Sheskey, P. & Quinn, M. *Handbook of Pharmaceutical Excipients* (Libros Digitales-Pharmaceutical Press, 2009).
41. Siddiqui, M. R., AlOthman, Z. A. & Rahman, N. Analytical techniques in pharmaceutical analysis: A review. *Arab. J. Chem.* **10**, S1409–S1421 (2017).
42. Al-Achi, A. J. & Kanade, A. Y. Determining sucrose concentration in syrups by pharmaceutical methods. *J. Clin. Pharmacol. Biopharmaceut.* **8**, 1 (2019).
43. Poka, M. S., Milne, M., Wessels, A. & Aucamp, M. Sugars and polyols of natural origin as carriers for solubility and dissolution enhancement. *Pharmaceutics* **15**(11), 2557 (2023).
44. Wang, K. et al. Symptomatic treatment of the cough in whooping cough. *Cochrane Database Syst. Rev.* **2014**(9), CD003257 (2014).
45. International Organization for Standardization (ISO) (2017) ISO/IEC 17025 - General requirements for the competence of testing and calibration laboratories. Geneva
46. Harris, D. C. *Quantitative Chemical Analysis* (Macmillan, 2010).

47. Kolling, W. M. (2004). Handbook of pharmaceutical excipients. American Journal of Pharmaceutical Education, 68, BF1.
48. Lide, D. R. *CRC Handbook of Chemistry and Physics: A Ready-Reference Book of Chemical and Physical Data* (CRC Press, 1995).
49. Gibson, M. Pharmaceutical preformulation and formulation. *Drugs Pharm Sci* **199**, 199 (2001).
50. Remington, J. P. *Remington: The Science and Practice of Pharmacy* Vol. 1 (Lippincott Williams & Wilkins, 2006).
51. Han, X. et al. Microfluidic microwave sensor loaded with star-slotted patch for edible oil quality inspection. *Sensors* **22**(17), 6410 (2022).
52. Sattari, M. A. & Hayati, M. Accurate and non-contact measurement of volume percentages of oil-water fluids using microstrip sensors independent of the volume of sample using artificial neural network. *Flow Meas. Instrum.* **97**, 102621 (2024).
53. Abdulsattar, R. K., Sadeq, S. M., Elwi, T. A., Abdul Hassain, Z. A. & Muhsin, M. Y. Artificial neural network approach for estimation of moisture content in crude oil by using a microwave sensor. *Int. J. Microw. Opt. Technol.* **18**(5), 511 (2023).
54. Armghan, A., Alanazi, T. M., Altaf, A. & Haq, T. Characterization of dielectric substrates using dual band microwave sensor. *IEEE Access* **9**, 62779–62787 (2021).
55. Zonouri, S. A., Ali Alsailawi, H. & Mudhafar, M. A high-sensitivity Wilkinson power divider sensor for detecting dielectric properties in edible oils. *Sens. Imaging* **26**(1), 1–34 (2025).
56. Zonouri, S. A., Amirabadi, P. A. & Sarabi, H. G. Microwave sensing of honey composition: a triplexer-based approach for sucrose and proline measurement. *Meas. Sci. Technol.* **36**(5), 055102 (2025).
57. Kandwal, A. et al. A dual-band microwave sensor for glucose measurements utilizing an enclosed split ring metamaterial-based array. *Eng. Sci. Technol. Int. J.* **62**, 101947 (2025).

Author contributions

Seyed Abed Zonouri: Software, Validation, Formal analysis, Methodology, Conceptualization, Supervision, Project administration Saeed Mehdipourbashi: writing, original draft preparation Mazdak Rad Malekshahi: Revising, Validation, Formal analysis All authors have read and agreed to the published version of the manuscript.

Declarations

Competing interests

The authors declare no competing interests.

Additional information

Correspondence and requests for materials should be addressed to S.A.Z.

Reprints and permissions information is available at www.nature.com/reprints.

Publisher's note Springer Nature remains neutral with regard to jurisdictional claims in published maps and institutional affiliations.